Available online at www.sciencedirect.com
ScienceDirect
Journal of Power Sources 158 (2006) 1538–1543
JOURNAL OF POWER SOURCES
www.elsevier.com/locate/jpowsour

Short communication

Nano SnO_2–Al_2O_3 mixed oxide and SnO_2–Al_2O_3–carbon composite oxides as new and novel electrodes for supercapacitor applications

M. Jayalakshmi, N. Venugopal, K. Phani Raja, M. Mohan Rao *

Inorganic Chemistry Division, Indian Institute of Chemical Technology, Uppal Road, Hyderabad 500 007, India

Received 6 October 2005; received in revised form 26 October 2005; accepted 26 October 2005
Available online 7 December 2005

Abstract

New nano-materials like SnO_2–Al_2O_3 and SnO_2–Al_2O_3–carbon were synthesized by a single step hydrothermal method in searching for novel mixed oxides with high electrochemical double layer capacitance. A SnO_2–Al_2O_3–carbon sample was calcined at 600 °C and tested for its performance. The source of carbon was tetrapropyl ammonium hydroxide. The capacitive behavior of SnO_2 was compared to the performance of SnO_2–Al_2O_3, SnO_2–Al_2O_3–carbon and calcined SnO_2–Al_2O_3–carbon using the techniques of cyclic voltammetry, double potential step, chronopotentiometry and E–log I polarization. In 0.1 M NaCl solutions, SnO_2–Al_2O_3 gave the best performance with a value of 119 Fg^{-1} and cycled 1000 times. The nano-material mixed oxides were characterized by TEM, XRD, ICP-AES and SEM-EDAX.

Keywords: Nano; Mixed metal oxides; SnO_2–Al_2O_3; SnO_2–Al_2O_3–carbon; Electrochemical capacitor; Hydrothermal method

1. Introduction

A recently rejuvenated interest in the development of super or ultra or electrochemical double layer capacitors (EDLC) is due to the power requirements of a number of applications that have exceeded the capability of batteries available in the market to-day. As an alternative power source, EDLC is being intensively investigated in the United States, Japan, Europe and Russia. To increase the power delivery at least by one order of magnitude higher than existing capacitors, metal oxides and mixed metal oxides has been introduced as electrodes which also deliver pseudo-capacitance. For an ideal double layer capacitor, the charge is transferred into the double layer and there are no Faradaic reactions between the solid material and the electrolyte. In this case, the capacitance is constant and independent of voltage. On the other hand, for capacitors that use metal oxides, pseudo-capacitance due to Faradaic reactions between the solid material and the electrolyte arises and it is voltage dependent. The double layer capacitance has a typical value of 10–40 $\mu F\,cm^{-2}$ for a real surface, while pseudo-capacitance may be 10–100 times greater. Prototypes made of ruthenium and tantalum oxides have been highly successful and are commercialized [1]. As ruthenium is highly expensive, alternative metal oxides are explored.

Lead Pb/Ru pyrochlore ($Pb_2Ru_2O_{6.5}$) was synthesized as a new electrode material for aqueous electrolyte capacitors and the performance was similar to ruthenium oxide electrodes [2]. Nano-porous vanadium oxide (V_2O_5) prepared by the sol–gel method was shown to have a maximum capacitance of 214 Fg^{-1} obtained at a scan rate of 5 mV s^{-1} in 2 M KCl [3]. Studies on a solid-state capacitor based on Ppy (polypyrrole)/Al_2O_3/Al prepared by the constant current method revealed that three stages, namely the formation of Al_2O_3 and the nucleation of Ppy within the pores of Al_2O_3, the propagation of Ppy on the Al_2O_3 barrier layer and the over-oxidation of Ppy located in the pores of Al_2O_3, play a vital role on the performance of the capacitor [4]. Amorphous MnO_2 was synthesized using the sol–gel method and a maximum capacitance of 110 Fg^{-1} was obtained at a scan rate of 5 mV s^{-1} in 2 M NaCl solution [5]. MnO_2 grown from $MnSO_4$ solutions mixed with acetate based electrolytes has been studied for electrochemical capacitor applications and has shown a consistent decrease in specific capacitance from 260 to 50 Fg^{-1} as the material thickness increases [6]. Hydrous IrO_2 has been found to perform in electrochemical capacitor

* Corresponding author. Tel.: +91 40 27193510; fax: +91 40 27160921.
E-mail address: mandapati@iict.res.in (M.M. Rao).

0378-7753/$ – see front matter © 2005 Elsevier B.V. All rights reserved.
doi:10.1016/j.jpowsour.2005.10.091

applications with a specific capacitance close to 550 Fg^{-1} [7]. $SrCoO_{2.5}$ was tested to be a potential active electrode material for an electrochemical capacitor and a specific capacitance of 168.5 Fg^{-1} could be obtained in the range of 0.1–0.7 V [8]. Sb-doped SnO_2 and composite electrodes of SnO_2 in combination with ruthenium oxide and iron oxide have been studied for their suitability as electrodes for supercapacitors and SnO_2–Fe_3O_4 was shown to have specific capacitance comparable with the carbon electrodes but with a much higher capacitance density [9]. Pseudo-capacitive behavior of $Ti/RhO_x + Co_3O_4$ electrodes in acidic medium revealed that the electrochemical performance depends on the composition of the oxides. A decrease in the voltammetric charge with cycle number was observed for 5–10 mol% Rh electrodes which has been related to the cathodic dissolution of CoO [10]. NiO/RuO_2 composite materials were prepared for use in electrochemical capacitors (ECs) by a co-precipitation method and a maximum specific capacitance of 210 Fg^{-1} was obtained for NiO-based composite electrode with 10 wt.% RuO_2 in the voltage range from −0.4 to 0.5 V in 1 M KOH solution [11]. $Ir_{0.3}Mn_{0.7}O_2$ electrodes perform well in electrochemical capacitor applications with a specific capacitance close to 550 Fg^{-1} [12].

Nano-crystalline metal oxides that have high surface area, high conductivity, electrochemical stability and pseudo-capacitive behavior can be highly significant in this aspect. Capacitors based on activated carbon materials have been successfully commercialized using non-aqueous electrolytes to increase the operating potential of the devices. To combine mixed metal oxides and carbon in a single electrode as a composite nano-material could achieve all the benefits. Alumina is a widely used support due to the good mechanical properties of alumina and its ability to disperse the active oxide phase. Substrate–metal (Al_2O_3/Pd) charge transfer induced by the dipoles at the interface was proven to play a crucial role in increasing the CO adsorption and dissociation [13]. In this communication, we synthesized a SnO_2–Al_2O_3 mixed oxide and a SnO_2–Al_2O_3–carbon composite mixed oxide by a single step hydrothermal method. Urea was used as the hydrolytic agent. These nano-materials were characterized by XRD, TEM, ICP-AES and SEM-EDAX. Electrochemical characterization by cyclic voltammetry, double step chronopotentiometry and E versus $\log I$ polarization measurements were done to evaluate the use of these nano-materials as potential electrodes for supercapacitor applications. The electrochemical performance of single SnO_2 was compared to these composite electrodes under identical conditions to understand the beneficial effects of Al_2O_3 and carbon.

2. Experimental

Chemical syntheses of all the mixed oxides were done in a single step hydrothermal process involving urea as the hydrolytic agent. SnO_2–Al_2O_3–carbon was calcined at 600 °C and the sample was tested for electrochemical performance. SnO_2–Al_2O_3, SnO_2–Al_2O_3–carbon and calcined SnO_2–Al_2O_3–carbon oxides were designated as Sn–Al, Sn–Al–C and Sn–Al–CC, respectively.

2.1. Hydrothermal synthesis

2.1.1. SnO_2–Al_2O_3

The reactants for this nano-oxides were $SnCl_2 \cdot 2H_2O$ (0.05 mol), $Al(NO_3)_3 \cdot 9H_2O$ (0.05 mol) dissolved in 250 ml of water and then, urea (0.4 mol) was added to the homogeneous mixture and transferred to an autoclave and allowed to reach 180 °C within an hour (ramp time). The reaction was kept at this temperature for 2 h (soak time) with an in situ pressure of 12 atm. After 2 h, it was cooled down slowly to room temperature. The product was filtered, washed with acetone and dried at 110 °C in a hot air oven. The initial pH of the experimental solution was highly acidic (pH 1) and the final pH was alkaline (pH 9.5).

2.1.2. SnO_2–Al_2O_3–carbon

For this sample, the procedure was the same as above with an exception. As the carbon source, 0.05 mol of tetrapropylammonium hydroxide (Fluka, Germany) was added which produces a cloudy white precipitate. A similar method was reported recently to incorporate carbon atoms to TiO_2 [14]. The initial pH of the experimental solution was acidic (pH 4) and the final pH was alkaline (pH 11). A part of this sample was subjected to calcinations at 600 °C for 3 h.

2.1.3. SnO_2

For this nano-oxide, initially SnO was synthesized and then calcined. The reactants were $SnCl_2 \cdot 2H_2O$ (0.05 mol) and urea (0.2 mol) and the same procedure was repeated as above. SnO nanoparticles were again calcined at 600 C for 3 h to get SnO_2.

2.2. Instrumentation

All electrochemical experiments were conducted with a PGSTAT 30 Autolab system (Ecochemie, Utrecht, The Netherlands). It was connected to a PC running with Eco-Chemie GPES software. GPES software was used for all electrochemical data analysis. The reference electrode was Ag/AgCl (3 M KCl) and the counter electrode was a platinum foil supplied along with the instrument. Paraffin impregnated graphite electrodes (PIGE) were used as working electrodes with the surface immobilized with the active electrode materials. A few micrograms of mixed oxide nano-particles were placed on a clean glass plate and the surface of PIGE electrode was pressed over the nano-material which would mechanically transfer the nano-particles to the tip of the electrode.

Powder XRD data of the samples were obtained by means of a Siemens D 5000 X-ray diffractometer with Bragg–Brentano geometry and having Cu Kα radiation (λ = 1.5418 Å). The samples were scanned for 2θ values in the range from 2° to 80°. Transmission electron microscope (TEM) images were obtained with a PHILIPS Tecnai-12 FEI instrument operated at an accelerating voltage of 100 kV. SEM-EDAX analysis was done using scanning electron microscope, Leo 440 (Germany) equipped with an Econ 4 detector (EDAX, USA). ICP-AES analysis was

done in IRIS Intrepid II XDL model from Thermo Electronic Corporation, USA

3. Results and discussion

3.1. Characterization of nano-materials

An XRD pattern of hydrothermally synthesized Sn–Al sample is shown in Fig. 1. The XRD pattern matches the standard file of SnO_2 (JCPDS card no. 21-1250). The pattern proves the crystalline nature of SnO_2 nano-particles compared to $AlOOH/Al_2O_3$ which was highly amorphous as indicated by the absence of peaks in the XRD. Fig. 2 shows the TEM images of SnO_2–Al_2O_3 nanoparticles. The amorphous phase Al_2O_3 was clearly shown by the cloudy alignment of super fine particles while the darker spherical particles scattered over the cloudy backdrop were the finer crystalline SnO_2 nano-particles.

For the carbon-doped mixed oxide samples, the XRD patterns appear in a similar fashion with no telltale peaks for either Al_2O_3 or carbon. SEM-EDAX and ICP-AES elemental analysis for the Sn–Al sample was as follows: 11.21% Al; 35.82% Sn. Analysis of the Sn–Al–C sample confirmed the presence of carbon

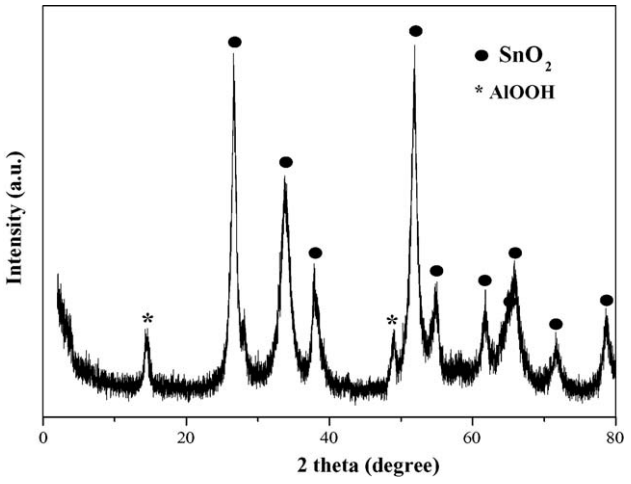

Fig. 1. XRD pattern of as prepared SnO_2–Al_2O_3 by hydrothermal method.

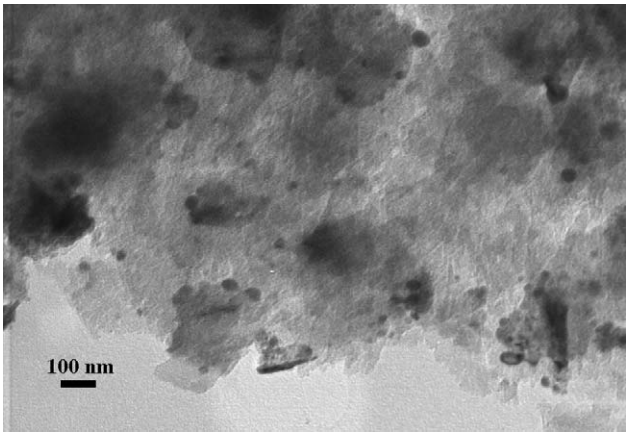

Fig. 2. TEM image of as prepared SnO_2–Al_2O_3 by hydrothermal method.

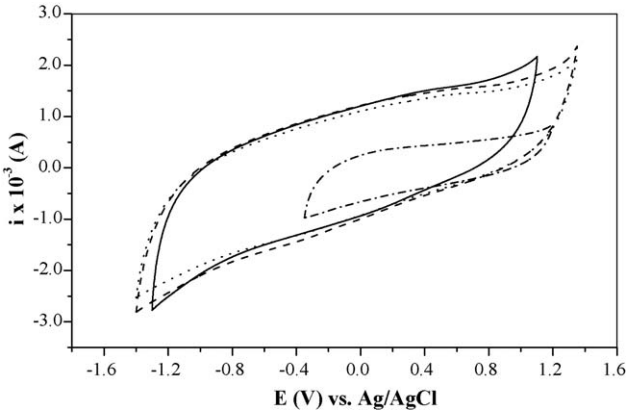

Fig. 3. Cyclic voltammograms of oxide nanoparticles immobilized on PIGE electrode in 0.1 M NaCl solution; scan rate 100 mVs^{-1}; - · -, SnO_2; —, Sn–Al; . . ., Sn–Al–C; - - -, Sn–Al–CC.

(3.9% C). The TEM image also confirms the presence of amorphous Al_2O_3 as the matrix with nanocrystalline SnO_2 dispersed within it.

3.2. Electrochemical characterization

Cyclic voltammograms (CVs) obtained for nano SnO_2, SnO_2–Al_2O_3, SnO_2–Al_2O_3–carbon and calcined SnO_2–Al_2O_3–carbon oxides (designated as Sn–Al, Sn–Al–C and Sn–Al–CC, respectively) are shown in Fig. 3. The electrochemical response was stabilized after continuous cycling of 1000 scans. All the samples exhibit capacitive behavior by displaying almost rectangular shaped *I–V* curves, which is characteristic of electrodes responding as electrochemical double layer capacitors. The most striking feature among the four CVs shown in Fig. 3 is the CV for SnO_2; it has a smaller potential window and charges flowing under the CV curve were lower. Hence, in the new mixed oxide consisting of SnO_2 and SnO_2–Al_2O_3, there were two factors that signaled the better performance, namely the potential window and an increasing charge due to the presence of Al_2O_3 in the mixed oxide that seems to induce greater charge separation at the interface, a important criteria for an electrode to acts as electrochemical capacitor. The electrochemical responses of Sn–Al–C and Sn–Al–CC samples did not differ much from Sn–Al except for a slight extension of the potential window on either side. Table 1 shows the specific capacitances calculated for the subsequent cycles from 1st, 100th, 500th, 1000th scans for the four oxides;

Table 1
Specific capacitance values calculated from the cyclic voltammograms for the 1000 scans; scan rate, 100 mVs^{-1}

Cycle no.	Specific capacitance (Fg^{-1})			
	SnO_2	Sn–Al	Sn–Al–C	Sn–Al–CC
1	34.85	88.39	68.18	67.49
100	34.90	88.90	69.27	78.84
500	34.91	88.71	78.29	86.51
1000	36.72	91.96	83.35	92.69

it can be seen that the specific capacitance values remain almost constant throughout the cycling except for minor variations. Out of the four oxides, Sn–Al, gives the best performance in all cycles while the Sn–Al–CC samples gradually increase their performance with cycling. Sn–Al–CC performs better than Sn–Al–C, and may be due to the increase in crystallinity upon calcination.

SnO_2 is a well-known semiconductor with an optical band gap of 3.6 eV. This optical band gap could be compared to the electrochemical band gap or (ΔV) which was calculated from the cyclic voltammetric curves by measuring the difference in potential in anodic and cathodic onset potential values [15]. A discussion of the relevance to ΔV in the electrochemical measurements of ZnS and that of band bending of CB and VB bands associated with the adsorption of positively and negatively charged ions at the semiconductor/solution interface was presented in our recent work [16]. Due to hydrogen overpotential and oxygen underpotential, SnO_2 has a ΔV value of 1.55 V; on the other hand, the Sn–Al sample ended up with a ΔV of 2.4 V due to both oxygen and hydrogen overpotentials. In the case of carbon added Sn–Al samples, both calcined and as prepared, the ΔV increased further due to the extension of overpotentials on either side of potential window.

The capacitive behavior of a nano-crystalline semiconductor electrode in contact with an aqueous electrolyte has been attributed to potential dependent intrinsic capacitance associated with the electronic state distribution. On exposure to dilute solutions, physisorption or chemisorption of metal ions, such as sodium ions, would create a layer of charges at the SnO_2 or SnO_2–Al_2O_3 surface within the Helmholtz layer. As a result, there exists a constant electrochemical potential between the working and counter electrode even under open-circuit conditions. As Al_2O_3 is an insulator, the charge separation at the interface initiated by the adsorption of ions could be more favorable for the mixed oxide than pure tin oxide. A space charge is created in general, when an insulator comes in contact with a semiconducting material. On application of an external bias, charge accumulation occurs being an indispensable prerequisite to align the band edges, and the adsorption of positive ions would shift the band edge (CB) in the positive direction while on the reverse negative scan, the adsorption of negative ions would shift the band edges (VB) in the negative direction. A positive shift of 0.2 V in the onset of the photocurrent for hydrogen production, due to the specific adsorption of Fe^{2+} ions, was reported for titania [17]. For a metal oxide semiconductor electrode, it was proven that the current onset potential can be assigned to the flat band potential and in the presence of double layer capacitance alone, the charging current will start at the flat band potential, becoming constant at a constant scan rate of potential [18]. Hence the unusual voltages observed for the mixed oxide and carbon added mixed oxides could be correlated to the upward band bending of the valence band (VB) band with concomitant downward band bending of the conduction band (CB) induced by the adsorption of ions at the interface.

In all the cyclic voltammograms in Fig. 2, the curves were not exactly rectangular as expected for a perfect double layer capacitor; in the case of an ideal capacitor, the equivalent circuit can be represented by a series combination of equivalent series resistance (R_D) and double layer capacitance (C_{dl}). The shape of the voltammogram was duly determined by the time constant, τ (RC) of the electrochemical cell. If $\tau(RC) \neq 0$, then the shape of the CV would be non-rectangular indicating a current containing a transient part as well as a steady state part. As τ becomes larger, the transient part lasts longer and hence more time is required to charge the capacitor resulting in the collapse of the rectangular current profile [19]. Other than the time constant, the pseudo-capacitance arising due to the electron transfer across the electrode/solution interface (as in the present study) would be coupled with the double layer capacitance; in such a situation, the equivalent series resistance arises from both the Faradic charge transfer resistance (R_F) and non-Faradic resistance (R_D) with the solution resistance (R_s) [20]. If one assumes the contribution from the solution resistance is negligible, the reasons for the slope of current–voltage curve could be due to: (1) increase in the particle size of the metal oxides due to the aggregation resulting in retarded transport of electrolyte ions; (2) a fast sweep rate, i.e the change in current with potential leads to a simultaneous fast drop in solution resistance; but the voltage across R_{ct} drops slowly due to the presence of the capacitor (C_{dl}); (3) a difference in particle sizes of nano-crystalline SnO_2 and amorphous alumina may create a difference in the wettability of the particles by the electrolyte, leading to a variation in local conductivity [21]. Any one or all of the above factors might have contributed to the non-rectangular profile of CV and with carefully planned experimentation, it is possible to evaluate this.

All the oxide samples were subjected to charge–discharge studies using double potential step chronopotentiograms. At a constant current rate of 500 μA, the samples were treated to 1000 cycles of charge–discharge and the results were tabulated (Table 2). Fig. 4 shows the typical plots obtained for a Sn–Al sample at the 1st, 250th, 1000th cycles. The curves are essentially straight lines, a trademark of capacitive charge–discharge behavior. The specific capacitance values increased gradually from the initial cycle, the highest value being that of the Sn–Al sample. The increasing order of performance was: Sn–Al > Sn–Al–CC > SnO_2 > Sn–Al–C. The maximum specific capacitance at the 1000th cycle for Sn–Al sample was 119 Fg^{-1} while the value was 92 Fg^{-1} from the CV measurements.

E–log I polarization curves obtained for the Sn–Al sample for the recorded 1st and 1000th scans are shown in Fig. 5. The polarization resistance R_p at E_{corr} at the positive and negative onset potentials give an idea of the reaction products deposited if any,

Table 2
Specific capacitance values calculated from the galvanostatic charge–discharge curves

Cycle no.	Specific capacitance (Fg^{-1})			
	SnO_2	Sn–Al	Sn–Al–C	Sn–Al–CC
1	87.92	111.77	74.40	79.36
250	90.25	112.78	81.92	89.20
1000	94.34	119.04	90.36	99.30

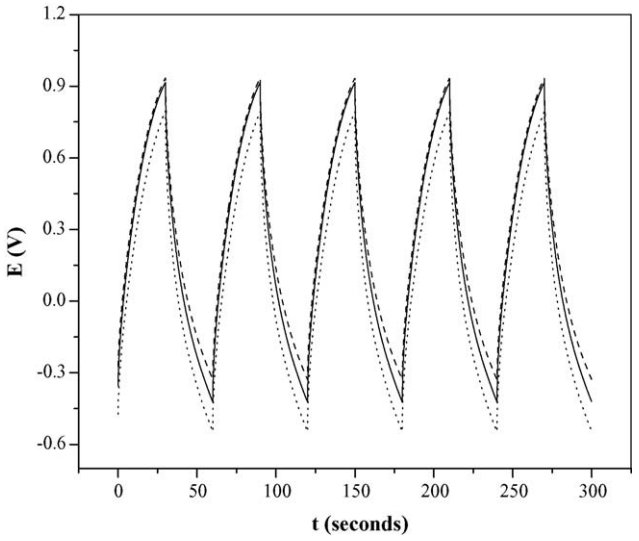

Fig. 4. Galvanostatic charge–discharge curves of Sn–Al sample at different cycles: · · ·, cycle 1; —, cycle 250; - - -, cycle 1000.

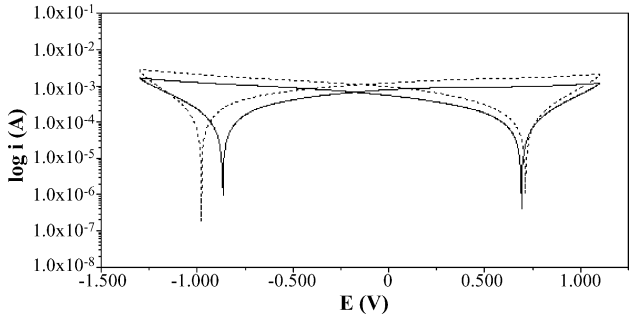

Fig. 5. E–log I polarization curves of Sn–Al sample derived from the cyclic voltammograms at cycle 1 —; cycle 1000 - - -.

especially in the case of Al_2O_3 on the surface of the electrode after persistent cycling. Table 3 shows the parameters derived for the four samples studied in this work. R_p values were obtained from the GPES software supplied with the potentiostat. They were calculated at $E_{m,H}$ and $E_{m,O}$ where $E_{m,H,}$ and $E_{m,O}$ denote the mixed potentials close to the hydrogen and oxygen evolution potentials, respectively. In general, R_p values obtained for the 1000th scan were less than during the first scan. As $R_p \sim 1/C_{dl}$, the observed trend looks valid though the difference in magnitude between the values at $E_{m,H}$ and $E_{m,O}$ in all the four oxides indicates that the hydrogen depolarization reaction occurs more easily than corresponding oxygen evolution.

Table 3
Polarization resistance (R_p) values from E–log I polarization curves

Sample	Cycle 1		Cycle 1000	
	$E_{m,H}$	$E_{m,O}$	$E_{m,H}$	$E_{m,O}$
SnO_2	638.7	1095	484.5	830.2
Sn–Al	682.3	907.2	409.6	572.8
Sn–Al–C	764.6	1051	450.4	690.9
Sn–Al–CC	520.7	735.9	428.5	652.9

Capacitances of both kinds are not unique but depend on the scan rate, solution concentration, pH, particle size, active surface area, applied current and time duration. Even the type of technique employed to synthesize makes a difference. SnO_2 prepared by the sol–gel method showed a value of 16 Fg^{-1} at the scan rate of 4 mV s^{-1} [22]; on the other hand, SnO_2 synthesized by electrochemical deposition showed a value of 285 Fg^{-1} at a scan rate of 10 mV s^{-1} [23]. For the nano-SnO electrode synthesized by the hydrothermal method, the specific capacitance value calculated for the stabilized 1000th cycle of the forward charging step of the chronopotentiogram was 24.58 Fg^{-1} and that during the backward discharging step was 17.3 Fg^{-1} [24]. An order of increase in capacitance values was obtained in the chronopotentiograms which are essentially a current step measurement where the output is linearly related to the voltage. On the other hand, in cyclic voltammograms, basically a potential step technique, the output current is an exponentially decaying one.

4. Conclusions

In this communication, we synthesized nano-SnO_2–Al_2O_3 and SnO_2–Al_2O_3–carbon composites via a simple single step hydrothermal route. In 0.1 M NaCl solutions, the electrochemical double layer capacitance of SnO_2–Al_2O_3 was much greater than of the pure SnO_2 and the electrode was electrochemically and chemically stable even after cycling1000 times. The performance of the carbon added composites was better than SnO_2 but lower than SnO_2–Al_2O_3. The expectation that added carbon would enhance the capacitance was not realised and further studies are required to understand this.

References

[1] A. Burke, J. Power Sources 91 (2000) 37.
[2] F. Cao, J. Prakash, J. Power Sources 92 (2001) 40.
[3] N. Ravinder Reddy, G. Ramana Reddy, J. Power Sources, in press.
[4] M.-L. Tsai, P.-J. Chenb, J.-S. Dob, J. Power Sources 133 (2004) 302.
[5] N.R. Reddy, G.R. Reddy, J. Power Sources 132 (2004) 315.
[6] J.N. Broughton, M.J. Brett, Electrochim. Acta 50 (2005) 4814 (and references therein).
[7] A.A.F. Grupioni, E. Arashiro, T.A.F. Lassali, Electrochim. Acta 48 (2002) 407.
[8] F. Xiao, X. Zhang, F. Hu, J. Zhang, Mater. Chem. Phy. 94 (2005) 221.
[9] N.-L. Wu, Mater. Chem. Phys. 75 (2002) 6.
[10] A.R. de Souza, E. Arashiro, H. Golveia, T.A.F. Lassali, Electrochim. Acta 49 (2004) 2015.
[11] X.M. Liu, X.G. Zhang, Electrochim. Acta 49 (2004) 229.
[12] A.A.F. Grupioni, E. Arashiro, T.A.F. Lassali, Electrochim. Acta 48 (2002) 407.
[13] N. Tsud, V. Johánek, I. Stará, K. Veltruská, V. Matolín, Surf. Sci. 467 (2000) 169.
[14] K.M. Reddy, B. Baruwati, M. Jayalakshmi, M.M. Rao, S.V. Manorama, J. Solid State Chem. 178 (2005) 3362.
[15] M. Al-Ibrahim, A. Konkin, H. Roth, D.A.M. Egbe, E. Klemm, U. Zhokhavets, G. Gobsch, S. Sensfuss, Thin Solid Films 474 (2005) 201.
[16] M. Jayalakshmi, M. Mohan Rao, J. Power Sources, in press.
[17] A. Bansai, J. Beach, R. Collins, O. Khaselev, J.A. Turner, Proceedings of the 1999 U.S. DOE Hydrogen Program Review, NREL/CP-570-26938.

[18] S.R. Morrison (Ed.), Electrochemistry at Semiconductor and Oxidized Metal Electrodes, Plenum Press, New York, 1980, p. 62;
M.S. Lee, I.C. Cheon, Y.I. Kim, Bull. Korean Chem. Soc. 24 (2003) 1155.
[19] M. Jayalakshmi, M.M. Rao, B.M. Choudary, Electrochem. Commun. 6 (2004) 1119.
[20] B.E. Conway, V. Birss, J. Wojtowicz, J. Power Sources 66 (1997) 1.
[21] K. Kierzek, E. Frackowiak, G. Lota, G. Gryglewicz, J. Machnikowski, Electrochim. Acta 49 (2004) 515.
[22] N.L. Wu, Mater. Chem. Phys. 75 (2002) 6.
[23] K.R. Prasad, N. Miura, Electrochem. Commun. 6 (2004) 849.
[24] M.M. Rao, M. Jayalaksmi, B.R. Reddy, S.S. Madhavendra, M.L. Kantam, Chem. Lett. 34 (2005) 712.